

# The Impact of Size Distribution Assumptions in a Bulk One-Moment Microphysics Scheme on Simulated Surface Precipitation and Storm Dynamics during a Low-Topped Supercell Case in Belgium

KWINTEN VAN WEVERBERG

*Department of Earth and Environmental Sciences, K.U.Leuven, Heverlee, Belgium, and Atmospheric Sciences Division, Brookhaven National Laboratory, Upton, New York*

NICOLE P. M. VAN LIPZIG

*Department of Earth and Environmental Sciences, K.U.Leuven, Heverlee, Belgium*

LAURENT DELOBBE

*Royal Meteorological Institute, Uccle, Belgium*

(Manuscript received 29 April 2010, in final form 5 October 2010)

## ABSTRACT

In this research the impact of modifying the size distribution assumptions of the precipitating hydrometeors in a bulk one-moment microphysics scheme on simulated surface precipitation and storm dynamics has been explored for long-lived low-topped supercells in Belgium. It was shown that weighting the largest precipitating ice species of the microphysics scheme to small graupel results in an increase of surface precipitation because of counteracting effects. On the one hand, the precipitation formation process slowed down, resulting in lower precipitation efficiency. On the other hand, latent heat release associated with freezing favored more intense storms. In contrast to previous studies finding decreased surface precipitation when graupel was present in the microphysics parameterization, storms were rather shallow in the authors' simulations. This left little time for graupel sublimation. The impact of size distribution assumptions of snow was found to be small, but more realistic size distribution assumptions of rain led to the strongest effect on surface precipitation. Cold pools shrunk because of weaker rain evaporation at the cold pool boundaries, leading to a decreased surface rain area.

## 1. Introduction

Proper simulation of deep moist convection in mid-latitude regions is still a difficult task, despite continuously improved physics and numerics over the past decades. Generally, the simulation of deep convection is associated with positive biases of the precipitation amounts and too vigorous updrafts (Weisman et al. 2008; Kain et al. 2008; Deng and Stauffer 2006). It remains challenging to point to a specific model deficiency responsible for this bias. As parameterized microphysical processes affect both the precipitation formation process and the thermodynamics

of convective systems, they have been thought to be a main contributor to overestimated surface rainfall.

Over the past decades, idealized studies with explicit cloud-scale models using bulk one-moment microphysics schemes (only predicting one moment; e.g., the mixing ratio) suggested that mainly the largest precipitating hydrometeor type (graupel or hail) has the largest influence on both the surface precipitation and the (thermo) dynamic processes within deep convective systems. Most studies were conducted for deep convection, and all found surface precipitation to increase as the size of hail or graupel increased (McCumber et al. 1991; Gilmore et al. 2004, hereafter GSR04; van den Heever and Cotton 2004, hereafter VC04). The precise nature of the impact was found to vary a lot among different studies, however. Some studies found a small impact on the accumulated surface precipitation—for example, VC04 and Cohen and

---

*Corresponding author address:* Kwinten Van Weverberg, Atmospheric Sciences Division, Brookhaven National Laboratory, Building 490-D, 75 Rutherford Drive, Upton, NY 11973-5000.  
E-mail: kvweverberg@bnl.gov.

McCaul (2006)—although the rainfall was spread over a larger area when the size of hail stones was decreased. McCumber et al. (1991) found a slightly more important sensitivity of surface precipitation of about 30% for idealized cases of tropical convection when replacing the large hail formulation in the Lin et al. (1983) microphysics scheme by small graupel. GSR04 found the surface precipitation to decrease enormously by a factor of 3–4 when the largest precipitating ice species was weighted toward small graupel instead of large hail for idealized cases of midlatitude supercell and multicell convection.

Also, the influence on storm dynamics was found to be significantly different among different studies. Some found stronger near-surface downdrafts and enhanced low-level cooling as the size of hail or graupel decreased, such as Cohen and McCaul (2006) or VC04. However, GSR04 found low-level downdrafts and cold pools to be weaker in experiments, including small graupel instead of large hail.

It should be mentioned that differences exist in the design of the experiments and in the microphysical schemes used among previously mentioned studies. GSR04 only varied the constant intercept and density of the hail variable, while McCumber et al. (1991) also varied the coefficients associated with the fall speed relations and hence had a somewhat more sophisticated experimental design. Furthermore, very few studies were conducted to investigate the impact of modifying particle size distribution (PSD) characteristics of other precipitating hydrometeors, being rain or snow, on the simulation of severe convection. GSR04, for example, mention that they have performed a number of sensitivity experiments on the snow and rain size distributions, but that they found overall little impact. Li et al. (2009) found the fixed rain intercept parameter in a one-moment bulk scheme to enhance evaporation and cold pool intensity as compared to a bin microphysics scheme.

Over the past decade, more sophisticated microphysics schemes are becoming available, predicting more moments of the hydrometeor distributions, such as the number concentration (zeroth moment; e.g., Ferrier 1994; Seifert and Beheng 2006), or the radar reflectivity (sixth moment; e.g., Milbrandt and Yau 2005), or separating distribution into several size categories instead of applying formulations on the bulk of the distribution (bin or spectral microphysical schemes; e.g., Kogan 1991; Khain et al. 1999; Ovtchinnikov and Kogan 2000). Similar sensitivity tests as presented here have been performed for such more sophisticated schemes (e.g., Morrison et al. 2009; Milbrandt and Yau 2006; Dawson et al. 2010). However, it remains unclear what the main drawbacks for many processes are of the way size distributions in one-moment bulk schemes are represented. Moreover, because of the computational cost of the more advanced schemes, one-moment bulk

microphysics schemes remain the workhorse in numerical weather prediction to this date, so sensitivity studies using such schemes are still very relevant.

In this research a systematic setup has been chosen to gradually implement modified size distribution assumptions of the rain, snow, and hail species in a simple one-moment bulk microphysical scheme within the Advanced Regional Prediction System (ARPS; Xue et al. 2000, 2001). All experiments are carried out for a case of extreme convection over Belgium, driven by strong shear conditions leading to a long-lived low-topped supercell. The main rationale for conducting this study is to understand if the differences in sensitivity found by previous research are caused by differences in the experimental design or different synoptic conditions. A further goal of this research is to investigate the sensitivity of moist processes to similar modifications to the snow and rain size distribution assumptions and to understand the physical mechanisms behind these sensitivities by means of extensive microphysical budget studies.

An overview of the model setup and synoptic and mesoscale aspects of the case studied is given in section 2. The experimental design is explained in section 3. In section 4 an overview of the results is given, discussing the storm dynamics and the microphysical budgets of each of the experiments performed. Concluding remarks are made in section 5.

## 2. Model setup and case description

### *a. ARPS description*

ARPS is a nonhydrostatic mesoscale meteorological model developed at the University of Oklahoma (Xue et al. 2000, 2001). The finite-difference equations of the model are discretized on an Arakawa C grid, employing a terrain-following coordinate in the vertical direction. Advection is solved with a fourth-order central differencing scheme and leapfrog time stepping. Land surface processes are parameterized following Noilhan and Planton (1989). The model was applied using one-way grid nesting with two levels. Data on a  $0.25^\circ$  horizontal resolution from the global operational model operated by the European Centre for Medium-Range Weather Forecasts (ECMWF) were used as initial conditions and as 6-hourly lateral boundary conditions for the model run with a 9-km grid spacing and a domain size of  $1620 \text{ km} \times 1620 \text{ km}$ . Within this domain, a smaller domain centered over Belgium and covering  $540 \text{ km} \times 540 \text{ km}$  with a 3-km resolution was nested. An overview of the model domain is shown in Fig. 1. In all simulations, 50 levels were used in the vertical with a spacing of 20 m near the surface, increasing to 1 km near the upper-model boundary, which was located

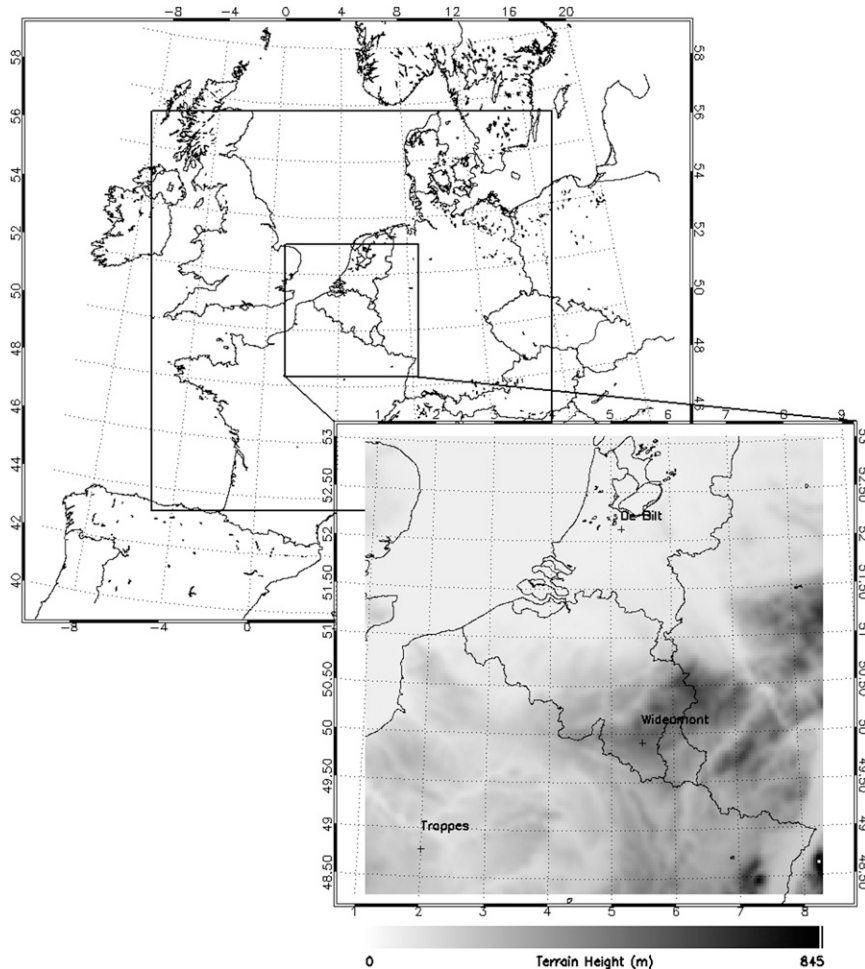


FIG. 1. Model domains used for all experiments. (top) Successive 9- and 3-km nested domains are denoted by bold rectangles. Inset shows the terrain height of the 3-km domain. Numbers in the margins indicate latitudes and longitudes.

at a 20-km altitude. All simulations were initialized with a 12-h spinup period, beginning at 1200 UTC on the previous day. All of the analysis in the following sections is concerned with the 0000–0000 UTC period, excluding the spinup period, if not stated otherwise. Turbulence was represented by the 1.5-order turbulent kinetic energy (TKE) model, and Sun and Chang (1986) parameterization for the convective boundary layer. The Kain–Fritsch (Kain and Fritsch 1993) cumulus parameterization was used in the largest domain, while no cumulus convection parameterization was used in the smaller domain. Cloud microphysics was parameterized following Lin et al. (1983), including five hydrometeor types (cloud water, cloud ice, rainwater, snow, and hail) in both the large and small domains. To suppress numerical noise, a fourth-order monotonic computational mixing scheme was applied, following Xue (2000).

### b. Case description

During the afternoon of 1 October 2006, several tornadic supercell thunderstorms developed over northern France and moved over Belgium, causing severe damage. Figure 2 provides an overview of the synoptic conditions at 1200 UTC. A trough at the 500-hPa level extended over the British Isles with an upper-level low (ULL) across Ireland and a ridge extending from southern Europe to eastern Europe. Between the ULL and the ridge, a strong gradient was obvious, leading to the development of a strong jet streak with winds up to  $60 \text{ m s}^{-1}$  at 200 hPa. The left exit region of the jet streak was positioned over Belgium during the afternoon. At the surface, an occlusion, connected to a low pressure area beneath the ULL passed across Belgium during the morning preceding unstable air masses advected from northern France. While the

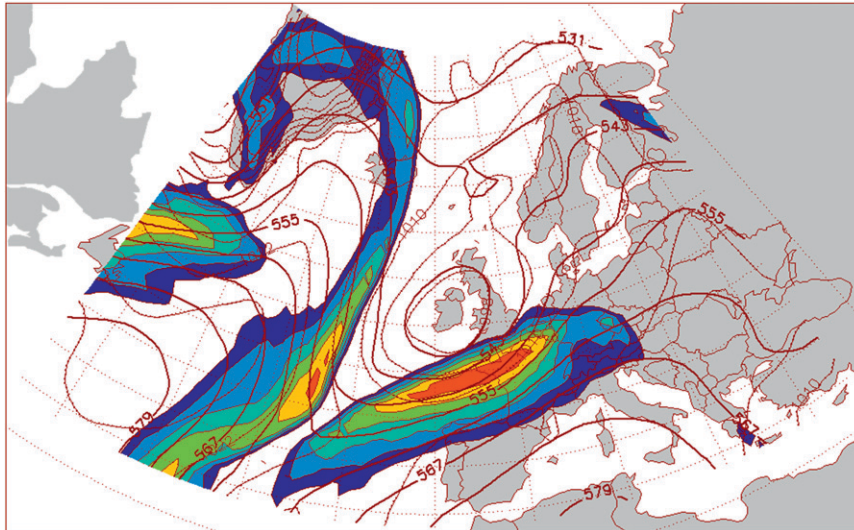


FIG. 2. ECMWF operational analysis at 1200 UTC 1 Oct 2006. Color shading indicates wind speed at 300 hPa (contours are drawn every 5 starting at  $30 \text{ m s}^{-1}$ ). Thick contour lines denote the 500-hPa geopotential level (contours are drawn every 5 dam), and thin contours denote the surface pressure (contours every 5 hPa).

thermodynamic instability, based on sounding data at 1200 UTC in Trappes (France, cross in Fig. 1), was only moderate with surface-based convective available potential energy (CAPE) values around  $1000 \text{ J kg}^{-1}$  and surface-based lifted index (LI) values around  $-3 \text{ K}$ , the kinematic environment exhibited substantial vertical wind shear. The low-level vertical wind shear reached values up to  $12 \text{ m s}^{-1}$ , while the 0–6-km shear amounted to  $28 \text{ m s}^{-1}$ . Storm relative helicity (SRH) values reached values up to  $210 \text{ m}^2 \text{ s}^{-2}$ . According to Groenemeijer and van Delden (2007), these are typical values across north-western Europe for tornado-producing thunderstorms. Onset of the supercell development in northern France was around 1400 UTC. Several supercell storms lasted more than 5 h and by then had reached the Netherlands and Germany. Localized precipitation accumulations up to 40 mm, hail (up to 2 cm), and several tornadoes were reported during this period.

### 3. Experimental design

Although many multimoment microphysics schemes have been developed over the past decade (e.g., Ferrier 1994; Milbrandt and Yau 2005; Seifert and Beheng 2006), most operational nonhydrostatic models still make use of the computationally less expensive one-moment schemes, which only have hydrometeor mass mixing ratios as prognostic variable. The microphysics scheme used in the control experiment of this study is the five-water species (cloud water, cloud ice, rain, snow, and hail) and the one-moment bulk scheme developed by Lin et al. (1983). All falling

hydrometeors are represented by exponential size distributions of the form

$$N_x(D) = N_{0x} \exp(-\lambda_x D_x), \quad (1)$$

where  $N$  is the number of particles per unit volume per unit size range,  $D_x$  is the maximum dimension of a particle, and  $N_{0x}$  and  $\lambda_x$  are the intercept and slope of the exponential size distribution, respectively. The subscript  $x$  denotes the water species (rain, snow, or hail). While the intercept parameter of all precipitating water species is assumed constant in the Lin et al. (1983) scheme (which is not a general feature of all one-moment bulk schemes), slope parameters, assuming all hydrometeors to be constant density spheres, are determined by

$$\lambda_x = \left( \frac{\pi \rho_x N_{0x}}{\rho q_x} \right)^{0.25}, \quad (2)$$

where  $\rho_x$  is the hydrometeor density,  $q_x$  is the hydrometeor mixing ratio, and  $\rho$  is the air density. An overview of specific formulations for the intercept, slope, density, and fall velocity for each of the precipitating water species in the Lin et al. (1983) scheme is provided in Table 1.

A number of sensitivity experiments have been designed to understand the implications of size distribution assumptions on the representation of moist processes in convection-resolving models. An overview of the impact of all sensitivity experiments on fall velocities for the precipitating hydrometeors is provided in Fig. 3, and a detailed description of the modifications of the slope and

TABLE 1. Overview of the formulations for all precipitating hydrometeors used in the control experiment (ExpH).

	Rain	Snow	Hail
$N_{0x}$	$N_{0r} = 0.08$ (Marshall and Palmer 1948)	$N_{0s} = 0.03$ (Gunn and Marshall 1958)	$N_{0h} = 0.0004$ (Federer and Waldvogel 1975)
$\lambda_x$	$\lambda_r = \left(\frac{\pi\rho_r N_{0r}}{\rho q_r}\right)^{0.25}$	$\lambda_s = \left(\frac{\pi\rho_s N_s}{\rho q_s}\right)^{0.25}$ (Lin et al. 1983)	$\lambda_h = \left(\frac{\pi\rho_h N_h}{\rho q_h}\right)^{0.25}$ (Lin et al. 1983)
$V_x$	$V_r = \frac{2115\Gamma(4+0.8)}{6\lambda_r^{0.8}} \left(\frac{\rho_0}{\rho}\right)^{1/2}$ (Liu and Orville 1969)	$V_s = \frac{152.93\Gamma(4+0.25)}{6\lambda_s^{0.25}} \left(\frac{\rho_0}{\rho}\right)^{1/2}$ (Locatelli and Hobbs 1974)	$V_h = \frac{\Gamma(4.5)}{6\lambda_h^{0.5}} \left(\frac{4g\rho_h}{3C_D\rho}\right)^{1/2}$ (Wisner et al. 1972)
$\rho_x$	$\rho_r = 1000 \text{ kg m}^{-3}$	$\rho_s = 100 \text{ kg m}^{-3}$	$\rho_h = 900 \text{ kg m}^{-3}$

intercept parameters, fall velocity, and density in all experiments is given in Table 2.

First of all, as indicated by GSR04, quantitative precipitation seems to be very sensitive to the way the largest

hydrometeor type, hail, is represented in the microphysical parameterizations. A first set of two experiments was designed to understand if the sensitivities found in idealized experiments only modifying the intercept parameter

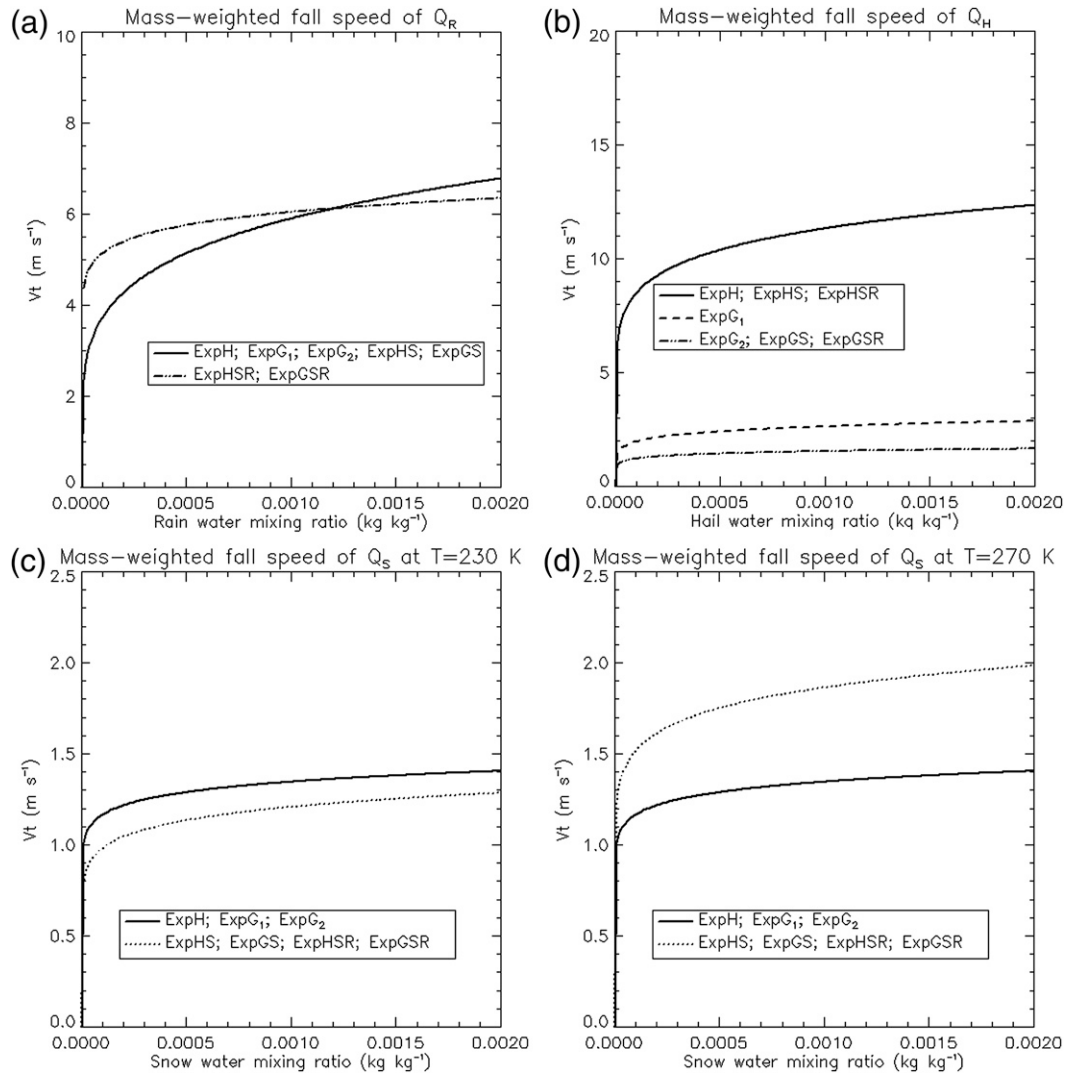


FIG. 3. Overview of mass-weighted fall speed relations vs mixing ratio of (a) rain, (b) graupel-hail, (c) cold snow (at  $T = 230 \text{ K}$ ); and (d) warm snow (at  $T = 270 \text{ K}$ ) according to all microphysics experiments included.

TABLE 2. Overview of all modifications made in the microphysics size distribution experiments. The × indicates modified formulations as compared to Table 1 (ExpH) for all precipitating hydrometeors, according to the respective formulas in the last column.

	ExpG <sub>1</sub>	ExpG <sub>2</sub>	ExpHS	ExpGS	ExpHSR	ExpGSR	Modification
$N_{0R}$					×	×	$N_{0r} = 0.07106(10^3 \rho q_r)^{0.648}$ (Zhang et al. 2008)
$\lambda_R$							—
$V_R$							—
$N_{0S}$			×	×	×	×	$N_{0s} = 0.02 \exp[0.12(T_0 - T)]$ (Houze et al. 1979)
$\lambda_S$			×	×	×	×	$\lambda_s = \left[ \frac{0.0074 N_{0s} \Gamma(2.1 + 1)}{\rho q_s} \right]^{1/(2.1+1)}$ (Locatelli and Hobbs 1974)
$V_S$			×	×	×	×	$V_s = \frac{209.60 \Gamma(0.28 + 2.1 + 1)}{\lambda_s^{0.28} \Gamma(2.1 + 1)}$ (Locatelli and Hobbs 1974)
$N_{0H}$	×	×		×		×	$N_{0h} = 4.0$ (GSR04)
$\rho_H$	×	×		×		×	$\rho_h = 400$ (GSR04)
$\lambda_H$		×		×		×	$\lambda_h = \left[ \frac{0.0702 N_{0h} \Gamma(2.7 + 1)}{\rho q_h} \right]^{1/(2.7+1)}$ (Locatelli and Hobbs 1974)
$V_H$		×		×		×	$V_h = \frac{234.42 \Gamma(0.37 + 2.7 + 1)}{\lambda_h^{0.37} \Gamma(2.7 + 1)}$ (Locatelli and Hobbs 1974)

and density of the largest precipitating hydrometeor (GSR04) could be reproduced for our simulation of a low-topped supercell in Belgium. Therefore, we performed two simulations: one using the intercept parameter and density value as in the original Lin et al. (1983) scheme, typical for large hail (referred to as ExpH); and one using a larger intercept parameter and lower density, identical to the values for small graupel in GSR04, referred to as ExpG<sub>1</sub>.

Two inconsistencies exist in the ExpG<sub>1</sub>, however. First, the calculation of  $\lambda_H$  for graupel is done assuming constant density spheres, which is contradicted by observational studies (e.g., Locatelli and Hobbs 1974). Second, the fall speed calculation of  $q_h$  in the graupel-weighted experiment is done using the original formulations in the Lin et al. (1983) scheme, following Wisner et al. (1972) for large hail. To understand the impact of these inconsistencies on the simulation results, a more advanced version of the graupel-weighted experiment was designed. This experiment (ExpG<sub>2</sub>) has an identical intercept parameter and density as in ExpG<sub>1</sub>, but the slope parameter for a constant density sphere and the fall speed for large hail were not retained. Using empirically derived mass–diameter and fall speed–diameter relations of the form  $m_x = a_{mx} D_x^{b_{mx}}$  and  $V_x = a_{vx} D_x^{b_{vx}}$ , respectively, one can express the slope parameter ( $\lambda_x$ ) and the fall speed ( $V_x$ ) as

$$\lambda_x = \left[ \frac{a_{mx} N_{0x} \Gamma(b_{mx} + 1)}{\rho q_x} \right]^{1/(b_{mx} + 1)} \quad \text{and} \quad (3)$$

$$V_x = \frac{a_{vx} \Gamma(b_{mx} + b_{vx} + 1)}{\lambda_x^{b_{vx}} \Gamma(b_{mx} + 1)}, \quad \text{respectively.} \quad (4)$$

The slope parameter and fall speed in ExpG<sub>2</sub> were calculated using Eqs. (3) and (4), respectively, and implementing

the empirically derived constants  $a_{mx}$ ,  $b_{mx}$ ,  $a_{vx}$ , and  $b_{vx}$  for dense lump graupel of Locatelli and Hobbs (1974).

A another focus of this investigation was to gain understanding of the consequences of having improved size distribution assumptions for the snow and rain variables. A third set of two experiments was identical to ExpH and ExpG<sub>2</sub>, apart from the fact that the snow size distribution assumptions were represented more realistically. For snow, too, a constant density sphere assumption is maintained in the original Lin et al. (1983) formulation, which is contradicted by observational data (e.g., Houze et al. 1979). Further, the assumption of a constant intercept parameter is not valid, as it is observed to vary over several orders of magnitude in the atmosphere (section 2.2 of Houze et al. 1979). Therefore, Eqs. (3) and (4) have been used to calculate  $\lambda_x$  and  $V_x$ , using the empirical relations derived by Locatelli and Hobbs (1974) for graupel-like snow. Further, we diagnosed the snow size distribution  $N_{0S}$  from air temperature, following Houze et al. (1979). In this way a set of two experiments was designed, referred to as ExpHS and ExpGS.

The last two size distribution experiments were identical to experiments ExpHS and ExpGS, except for the rain variable. As for the snow intercept parameter, the rain  $N_{0r}$  is known to vary over several orders of magnitude (e.g., Waldvogel 1974). Therefore, we diagnosed this parameter from the mixing ratio of rain, following Zhang et al. (2008). These last two experiments are referred to as ExpHSR and ExpGSR. Caution should be taken when comparing the results of the different experiments, as we incrementally introduced changes in a series of experiments. This means comparison of ExpHSR against ExpH is difficult, as it is some unknown combination of the changes made in the snow and the rain size distribution (Stein and Alpert

TABLE 3. Precipitation characteristics of all experiments (domain mean 24-h accumulated surface precipitation, domain maximum 24-h accumulated surface precipitation, and precipitation efficiency).

	Mean precipitation (mm)	Max precipitation (mm)	Precipitation efficiency
Analysis	1.6	35.0	
ExpH	3.1	42.5	30.7
ExpG <sub>1</sub>	3.5	34.4	28.6
ExpG <sub>2</sub>	3.4	37.0	24.9
ExpHS	3.0	42.0	30.4
ExpGS	3.3	44.7	24.8
ExpHSR	2.6	33.3	30.9
ExpGSR	2.7	28.5	24.5

1993). Therefore, we only compare pairs of experiments in which only one hydrometeor size distribution has been changed (i.e., ExpHSR against ExpHS, ExpHS against ExpH...).

**4. Results**

*a. Influence of graupel/hail size distribution*

Table 3 summarizes the 0000–0000 UTC temporal evolution of the surface precipitation characteristics for all experiments and as derived from combining weather radar and a dense network of rain gauges (1 per 135 km<sup>2</sup>), using a simple mean field bias adjustment (Goudenhoofd and Delobbe 2009). The radar used in this analysis is the C-band weather radar in Wideumont (indicated by the

asterisk in Fig. 1), operated by the Royal Meteorological Institute of Belgium, performing a 5-elevation reflectivity scan every 5 min. Figure 4 provides the 24-h (0000–0000 UTC) accumulated surface precipitation as analyzed and as simulated in ExpH. Mean absolute error using the mean field bias adjustment was found to be about 1.5 mm during a 4-yr verification against an independent set of rain gauge stations (Goudenhoofd and Delobbe 2009). To make a fair comparison between the analysis and the simulated precipitation fields, the analysis, having a spatial resolution of 600 m, has been aggregated to the ARPS grid. All simulated and observed 24-h accumulated surface precipitation estimates in the following paragraphs are for the region within a radius of 150 km from the radar location. From Fig. 4 and Table 3, it is clear that the 24-h accumulated surface precipitation is larger in ExpH than the analysis. Surface precipitation tends to increase as the largest frozen precipitation species is weighted toward small graupel. When only the intercept parameter and the density are modified (ExpG<sub>1</sub>), 24-h accumulated surface precipitation increases by 10%. Figure 5 shows the evolution over time of domain-averaged and maximum surface precipitation for the experiments including hail (Figs. 5a and 5c) and graupel (Figs. 5b and 5d). Domain-averaged precipitation fallout in the ExpG<sub>1</sub> tends to be slightly delayed but soon becomes larger as compared to the ExpH. Maximum precipitation intensity, however, always remains about 30% lower throughout the simulation in ExpG<sub>1</sub>.

It is not sure whether the increase in surface precipitation in ExpG<sub>1</sub> is primarily a thermodynamic effect of

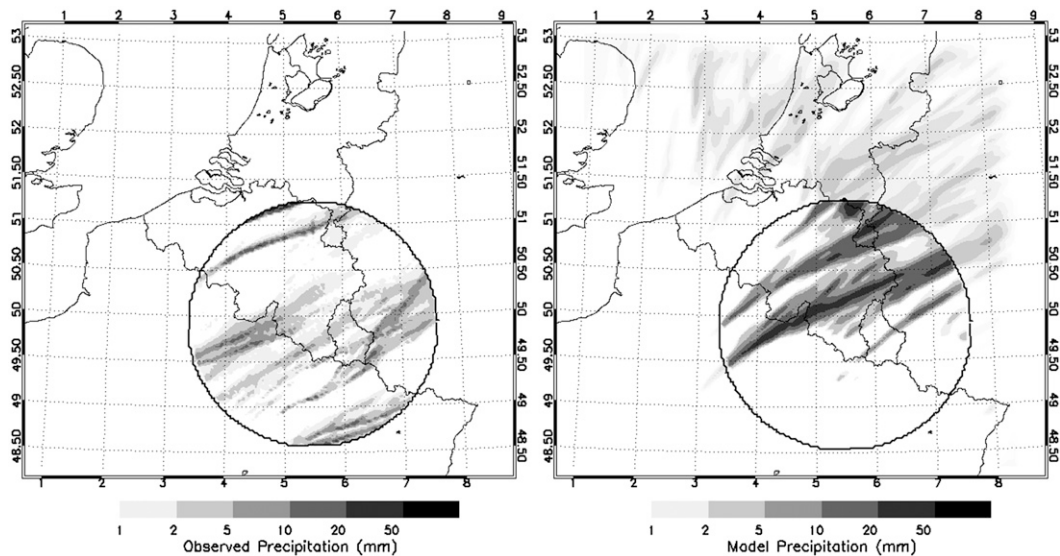


FIG. 4. Twenty-four-hour accumulated surface precipitation on 1 Oct 2006 as observed by (left) radar–rain gauge merging and (right) as simulated in the ExpH. Circle denotes a 150-km area around the position of the radar. All analyses throughout the text are concerned with this area. Therefore, surface precipitation shading outside the radar domain is dimmed.

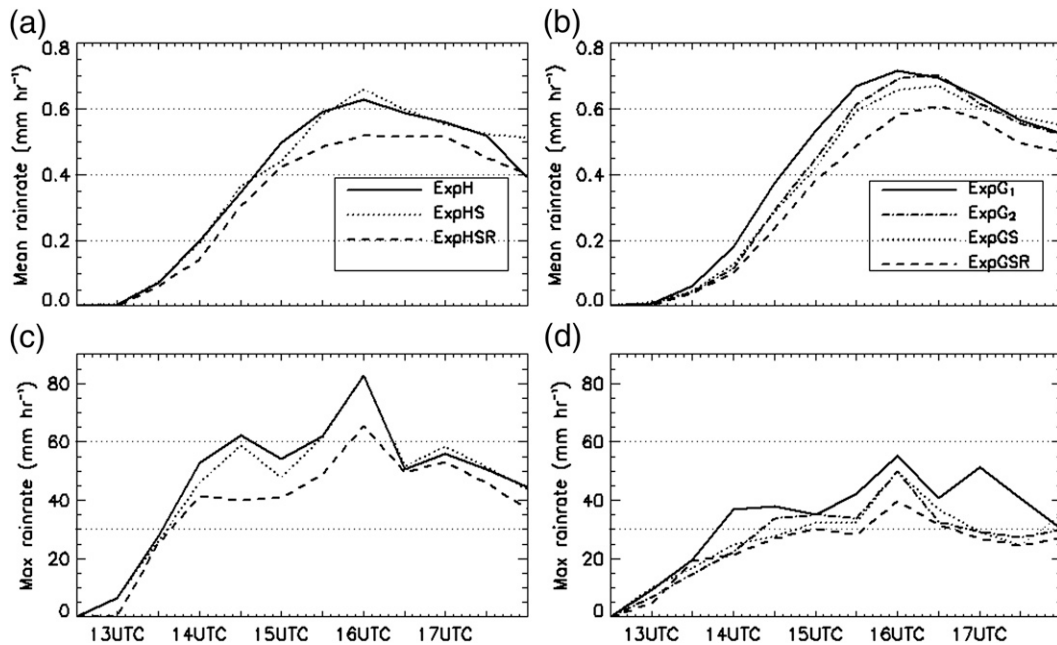


FIG. 5. (top) Time evolution of the domain-averaged hourly surface precipitation for the (a) hail-weighted experiments (ExpH, ExpHS, and ExpHSR) and (b) the graupel-weighted experiments (ExpG<sub>1</sub>, ExpG<sub>2</sub>, ExpGS, and ExpGSR) from 1230 to 1830 UTC. (bottom) Time evolution of the domain maximum hourly surface precipitation for the (c) hail- and (d) graupel-weighted experiments.

additional latent heat release associated with freezing and condensation processes or whether it is a pure microphysical conversion effect, increasing the precipitation efficiency leading to more efficient turnover of vapor to surface precipitation. Precipitation efficiency (PE), following Sui et al. (2007), is defined as

$$PE = \frac{P}{P_{wcdv} + P_{idpv} + P_{sdpv} + P_{intv}}, \quad (5)$$

where  $P$  is the surface precipitation rate ( $\text{kg s}^{-1}$ );  $P_{wcdv}$  is the vapor condensation;  $P_{idpv}$  and  $P_{sdpv}$  are the vapor deposition on cloud ice and snow, respectively; and  $P_{intv}$  is ice initiation. Vapor deposition on hail is not considered in the Lin et al. (1983) microphysics scheme. Values of PE for both cases and all experiments are given in Table 3. Clearly, PE is *decreased* in ExpG<sub>1</sub> as compared to ExpH. Figure 6 provides an overview of all conversion terms, aggregated over the domain covered by the radar and over the full precipitation period. While total vapor consumption by microphysical processes ( $P_{wcdv}$ ,  $P_{idpv}$ ,  $P_{sdpv}$ , and  $P_{intv}$ —all negative terms in Fig. 6a) increases by almost 20%, the surface precipitation increases by about 12%, resulting in slightly decreased PE [Eq. (5)]. This indicates that a larger portion of the condensate leaves the model by processes other than fallout to the surface in the ExpG<sub>1</sub> as compared to the ExpH. Indeed, a much larger portion of the condensate is returned to the vapor phase (positive

terms in Fig. 6a), mainly because of enhanced sublimation of graupel and rain evaporation ( $P_{vsbg}$  and  $P_{vevr}$ , Fig. 6a), which are associated with a longer residence time aloft of graupel and rain, respectively. Graupel falls slower than hail and hence there is more time for sublimation. Moreover, graupel is completely melted to rain at the freezing level, while hail often even reaches the surface, leaving more time for rain evaporation in experiments including graupel instead of large hail.

Strongly increased vapor consumption in combination with slightly decreased PE can explain the increased surface precipitation amounts in ExpG<sub>1</sub>. The increased vapor consumption is mainly associated with enhanced cloud water condensation (Fig. 6a). While it is hard to explain this increase from microphysical conversion processes alone, it might be revealing to analyze the thermodynamic effects of the presence of graupel as compared to large hail in the simulated convective storms. Latent heat release from all significant microphysical processes within storm updrafts containing graupel (ExpG<sub>1</sub>) and hail (ExpH) is provided in Fig. 7. As can be noticed in Fig. 6f, graupel growth occurs mainly through accretion of cloud droplets ( $P_{gacw}$ ), while this growth mechanism is of much less importance in ExpH. This growth mechanism provides an additional significant heat source within updrafts containing graupel (ExpG<sub>1</sub>). Furthermore, more heat is released due to the freezing of rain drops at contact with cloud ice ( $P_{iacr}$ ). Although cooling associated with

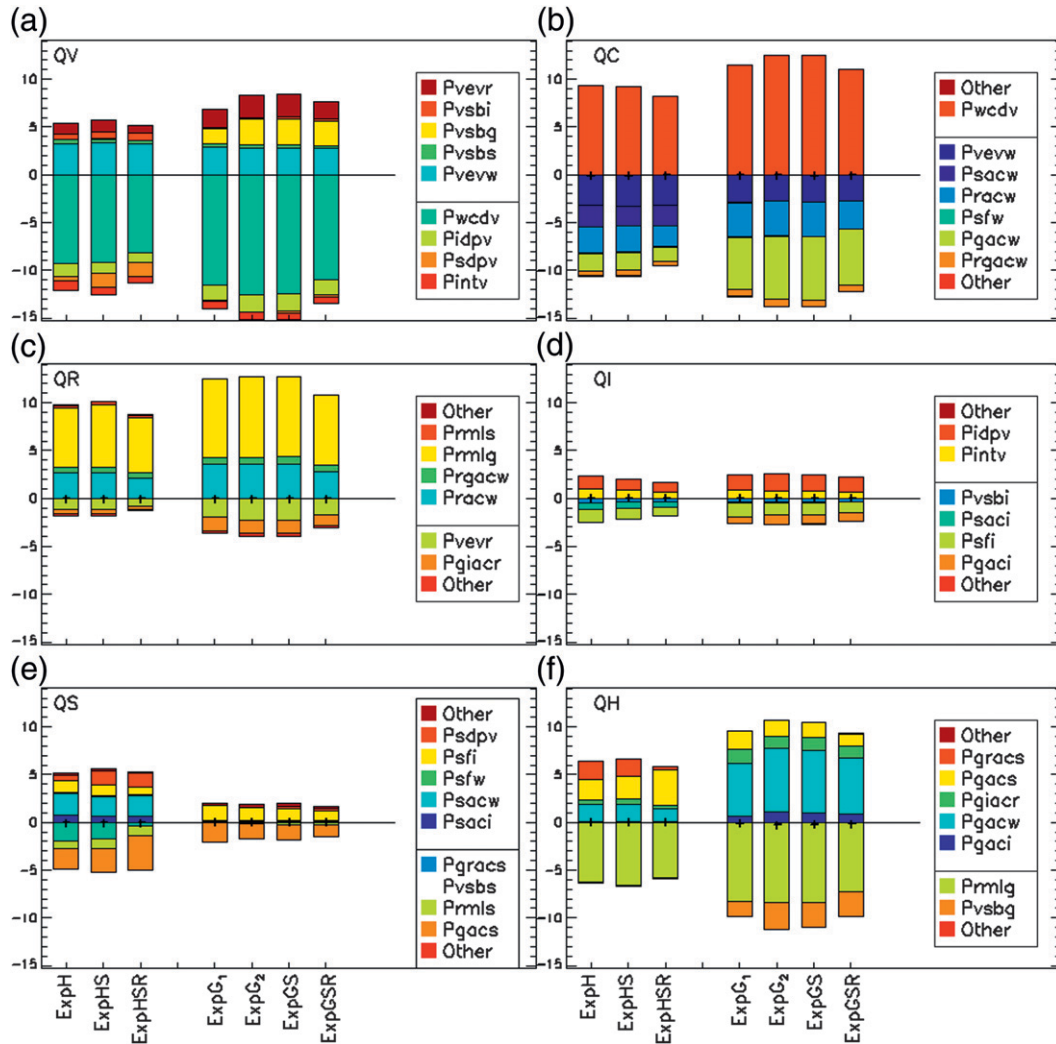


FIG. 6. Total production and loss ( $10^{11}$  kg) summed over the domain and over 24 h (0000–0000 UTC) during the shear-driven case for (top) (a)  $q_v$  and (b)  $q_c$ , (middle) (c)  $q_r$  and (d)  $q_i$ , and (bottom) (e)  $q_s$ , and (f)  $q_h$ , and for left to right experiments ExpH, ExpHS, ExpHSR, ExpG<sub>1</sub>, ExpG<sub>2</sub>, ExpGS, and ExpGSR. Naming convention is so that the species experiencing gain (loss) is represented by the first (last) letter. Third and fourth letters indicate the type of interaction: ev (evaporation), sb (sublimation), cd (condensation), dp (deposition), nt (initiation), ac (accretion), f (Bergeron process), and ml (melting). When three species are involved, the third letter indicates the accreting species.

melting of small graupel–hail (Prmlg) is larger in ExpG<sub>1</sub> as compared to ExpH, the net effect of enhanced Pgacw, Piacr, and Prmlg is a nonnegligible additional heat source in ExpG<sub>1</sub>, indicated by the gray line representing the net heat release in storm updrafts in Figs. 7a and 7b.

The additional latent heat release invokes a larger number of grid cells experiencing vertical velocities beyond  $1 \text{ m s}^{-1}$ , as can be seen from Fig. 8b, in which information on vertical velocities is summarized by means of contoured frequency by altitude diagrams (CFADs). This is consistent with the findings of GSR04, who found larger updraft volumes and intensities in experiments weighted toward small graupel. As updrafts are enhanced in ExpG<sub>1</sub>,

adiabatic processes of expansion and cooling become more intense, in turn leading to enhanced cloud water condensation (Pwcdv) and cloud ice deposition (Pidpv). Hence, increased freezing processes associated with the presence of graupel initiate a positive feedback mechanism leading to enhanced vapor consumption by microphysical processes. As the increased loss rates due to sublimation of graupel, leading to decreased PE, counteract this feedback mechanism, surface precipitation is only slightly increased, however.

The different relation between surface precipitation and the size distribution characteristics of the largest precipitating ice species in the experiments presented here and

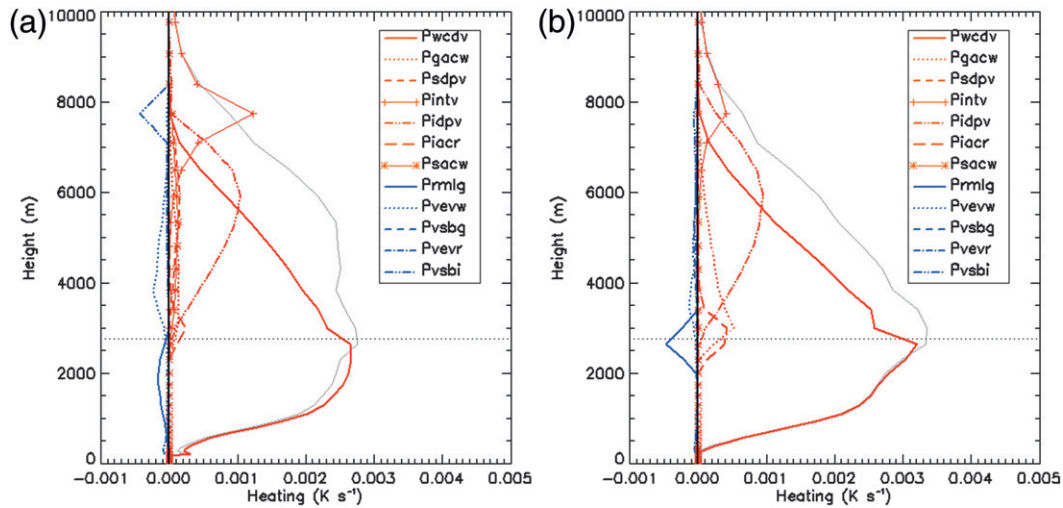


FIG. 7. Average latent heat release within updrafts (vertical velocity exceeding  $1 \text{ m s}^{-1}$ ) by all relevant microphysical processes over the precipitation period (1000–1800 UTC) for (a) ExpH and (b) ExpG<sub>1</sub>. Red lines are processes associated with warming, and blue lines are processes associated with cooling. Gray line denotes the net heating rate from all processes combined.

found in many other studies, such as McCumber et al. (1991) and GSR04, are probably due to differences in the thermodynamic environment. Vertical wind shear was mentioned by GSR04 as an important contribution to surface precipitation sensitivity when varying the size of hail or graupel. The stronger the wind shear in their experiments, the more surface precipitation was reduced when large hail was replaced by small graupel. This definitely explains part of the variability found in sensitivity among different previously conducted studies. Vertical wind shear in experiments conducted by McCumber et al. (1991) was much weaker (about  $1.5 \times 10^{-3} \text{ s}^{-1}$ ) as

compared to the vertical wind shear applied by GSR04 ( $6 \times 10^{-3} \text{ s}^{-1}$ ). Also, in Cohen and McCaul (2006) and VC04, vertical wind shear was somewhat lower as compared to GSR04 (about  $4 \times 10^{-3} \text{ s}^{-1}$ ). On the other hand, vertical wind shear in our simulations was very similar as compared to the experiments of GSR04.

A second parameter introducing variability in surface precipitation sensitivity might be the depth of storm systems. All previously mentioned studies finding decreased surface precipitation when graupel was included instead of large hail were associated with very deep storm systems, having cloud tops above 12 km, which are common in the

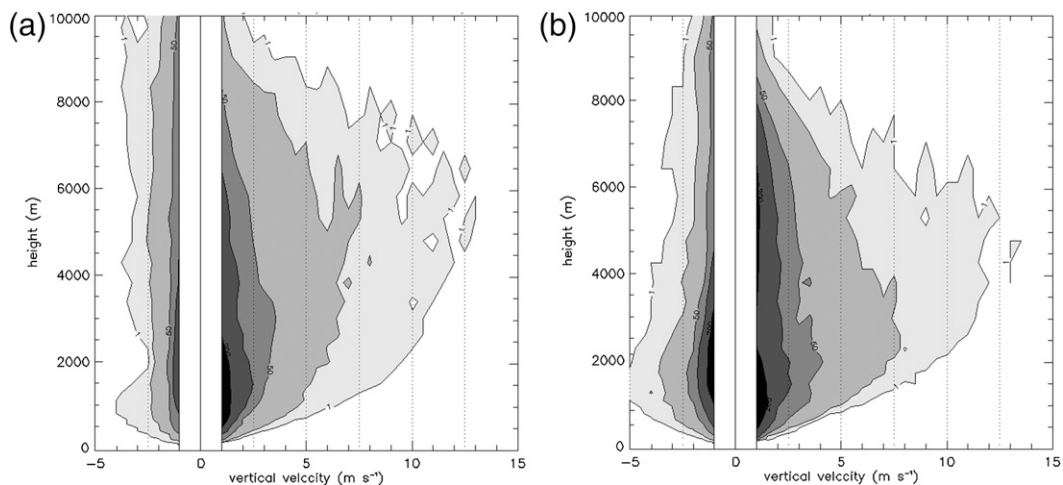


FIG. 8. The CFADS of the vertical velocity over the total domain for (a) ExpH and (b) ExpG<sub>1</sub> during the precipitation period (1000–1800 UTC). Shading indicates the number of grid cells within each velocity bin [ranging from 1 (light gray) to 200 grid cells (black)].

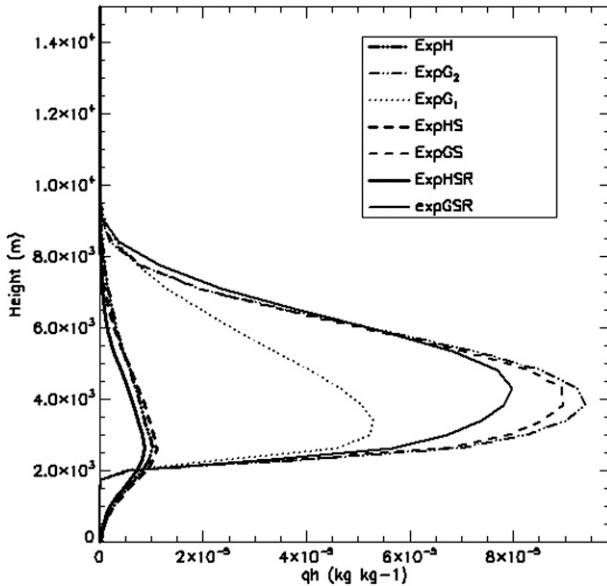


FIG. 9. Domain-averaged vertical profiles of graupel-hail from 1200 to 2000 UTC for all experiments.

North American warm season. Our simulations were conducted for low-topped supercell storms, however, with cloud tops below 8 km. The maximum in the mean vertical graupel profile was, for example, found at 9000 m in GSR04 as compared to 4000 m in our experiments (Fig. 9). This means that solid precipitation has to traverse a much longer distance through the atmosphere before reaching the melting level in simulations having deep storm systems, leaving more time for evaporation and sublimation. Indeed, while in ExpG<sub>1</sub> graupel loss due to sublimation is less than 20% of total graupel loss (Fig. 6f), the sublimation process in the similar N8p4 experiment of GSR04 accounts for almost half of the graupel loss (their Figs. 6 and 7). In their simulations the reduction in PE associated with the enhanced sublimation is likely to be much more important, so that it outweighs the enhanced latent heat release. Therefore, surface precipitation in their simulations is decreased in contrast to our findings. It should also be mentioned that many of the previously mentioned studies were based on rather short simulations; so it could be that the differences in surface precipitation in those studies would have become smaller if the simulations had lasted longer, as much of the precipitation could still have had time to fall out.

Significant differences among different studies exist also in the way downdrafts and cold pool characteristics are affected by varying the size distribution of the largest precipitation ice species. Some studies find stronger low-level downdrafts and cold pools in experiments weighted toward large hail (e.g., GSR04), while other studies find the stronger downdrafts and cold pools in experiments

weighted toward small graupel (e.g., VC04). Surface cold pools originate from intense evaporation and melting processes within storms, triggering strong downdrafts that are forced to diverge when reaching the surface. Cold pools are important features for storm development, as intense propagating cold pools are capable of inducing severe updrafts on their frontal boundary. Furthermore, they can aid in the development of baroclinically generated horizontal vorticity, which can in turn affect the tilt of the convective system. It is clear that in ExpG<sub>1</sub> downdrafts are much more vigorous below the melting level (Fig. 8b) as compared to ExpH (Fig. 8a). This can be explained by intense cooling by the melting of graupel and evaporation of rain within downdrafts below this level (Fig. 10b). The instantaneous melting of graupel when temperatures rise above zero induces a sudden cooling, which does not occur in the ExpH (Fig. 10a).

While lower atmosphere cooling and downdraft velocity is significantly affected by the presence of either hail or graupel, the difference in average surface cold temperature perturbation is fairly small, as can be inferred from Fig. 11. Figure 11 provides the time evolution of average and maximum cold pool intensity and cold pool size during all experiments. Equivalent potential temperature ( $\theta_E$ ) is approximated here as

$$\theta_E = \theta \exp\left(\frac{L_V w_S}{c_p T}\right), \quad (6)$$

where  $\theta$  is the potential temperature,  $L_V$  denotes the latent heat of vaporization,  $w_S$  is the saturated vapor mixing ratio,  $c_p$  is the specific heat of air at constant pressure, and  $T$  is the temperature. The equivalent potential temperature perturbation ( $\theta'_E$ ) is the departure from the domain wide horizontal average of  $\theta_E$ . The maximum cold pool  $\theta'_E$  is even surprisingly found in experiments weighted toward large hail. In those experiments, cold pools rapidly gain intensity mainly during the first hours of storm development, while cold pool buildup is slower in the graupel-weighted experiments (Figs. 11c and 11d). After 1500 UTC, differences in cold pool characteristics between ExpH and ExpG<sub>1</sub> disappear.

Figure 12 provides more detailed insight into the storm and cold pool structure in ExpH and ExpG<sub>1</sub>. These cross sections were taken through one of the two main supercell storms developing in the domain at 1500 UTC, when storms became mature. As can be derived from Figs. 11c and 11d, clear differences in cold pool characteristics between the ExpH and the ExpG<sub>1</sub> were still present at this time. From the horizontal cross sections, it is clear that intense cold pool areas are associated with the most vigorous downdrafts in the storms (denoted by the white

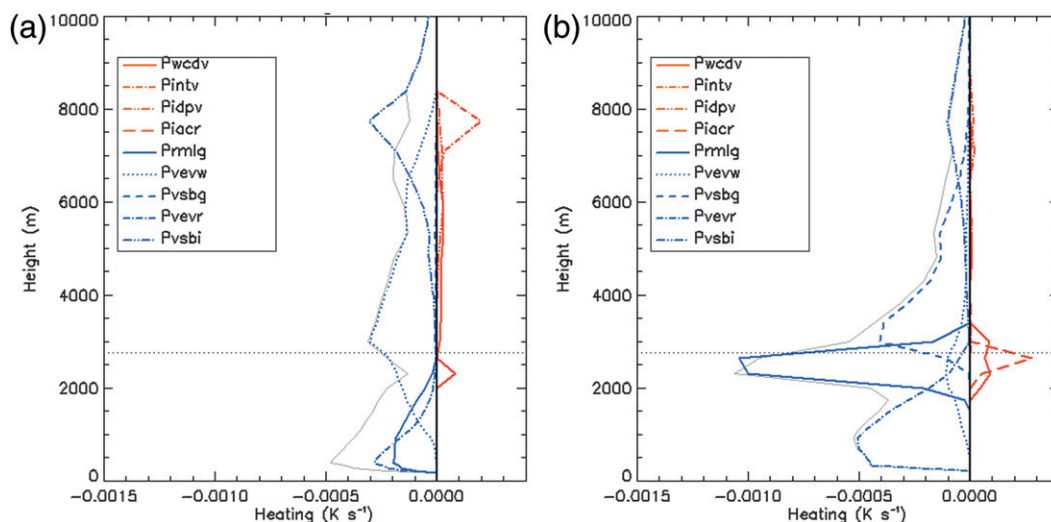


FIG. 10. Average latent heat release within downdrafts (vertical velocity  $< -1 \text{ m s}^{-1}$ ) by all relevant microphysical processes over the precipitation period (1000–1800 UTC) for (a) ExpH and (b) ExpG<sub>1</sub>. Red lines are processes associated with warming, and blue lines are processes associated with cooling. Gray line denotes the net heating rate from all processes combined.

contour). Both horizontal and vertical cross sections show that the most intense surface cold pools are found in the hail-weighted experiment, despite the more vigorous downdrafts in the graupel-weighted experiments discussed earlier. Those intense cold pool areas in the hail-weighted experiments are associated with intensively melting large hail reaching the surface (Figs. 12a and 12b). It is likely that downdrafts initiated at midtropospheric levels diffuse on their way down, resulting in somewhat broader but less intense cold pool areas, while it is the low-level cooling (within the lowest kilometers of the troposphere or so), associated with hail melt and rain evaporation, that is responsible for the most intense cold pools. Although midlevel cooling processes are most vigorous in ExpG<sub>1</sub>, near-surface cooling is dominant in ExpH, leading to intense but localized cold pools associated with hail melt. This is also consistent with differences found in literature among different studies. Indeed, in VC04, some graupel reaches the surface in all experiments, contributing to cooling due to melting down to the surface. In experiments by GSR04 as well as in our experiments, having the weaker cold pools in the graupel-weighted experiments, all graupel is melted well above the surface; hence, cooling due to melting ceases at a few kilometers above the surface, leading to smaller minimum cold pool perturbation temperatures in those experiments.

So far we only investigated the impact of modifying the hail intercept parameter and its density (ExpG<sub>1</sub>). However, this leads to an inconsistency, as the fall speed calculation is still based on the large hail formulation of Wisner et al. (1972). As graupel tends to fall slower than

hail of the same size (as it is not a constant density sphere), we applied an additional experiment to understand the impact of applying more consistent fall speed and size distribution assumptions (ExpG<sub>2</sub>). Surface precipitation in this experiment is almost unaffected as compared to ExpG<sub>1</sub> (Table 3; Fig. 5b). From Fig. 3b it is clear that in the ExpG<sub>2</sub>, graupel is falling even slower as compared to ExpG<sub>1</sub>, which leads the graupel amount to grow even larger (Fig. 9). As the graupel sediments slowly, more of it will sublimate (Pvsbg, Fig. 6f) to the vapor phase instead of falling toward the surface and melting to rain (Prmlg, Fig. 6f), which further decreases the precipitation efficiency (Table 3). However, even more condensation occurs in response to the increased latent heat release associated with the riming growth of graupel (Pgacw, Fig. 6f). The combination of both mechanisms yields almost no change in the surface precipitation.

#### b. Influence of snow and rain size distribution

In most [but not all, e.g., the Thompson et al. (2008) scheme] one-moment bulk microphysics schemes, snow has been represented as a constant density sphere and as having a constant intercept parameter. The impact of more realistic size distribution assumptions of snow on deep moist convection has rarely been investigated. Therefore, we further modified the setup of the experiments ExpH and ExpG<sub>2</sub> to use a temperature-dependent snow intercept parameter and assuming graupel-like snow instead of a constant density sphere for the slope parameter calculation (ExpHS and ExpGS). Accumulated surface precipitation in both experiments is very similar to their

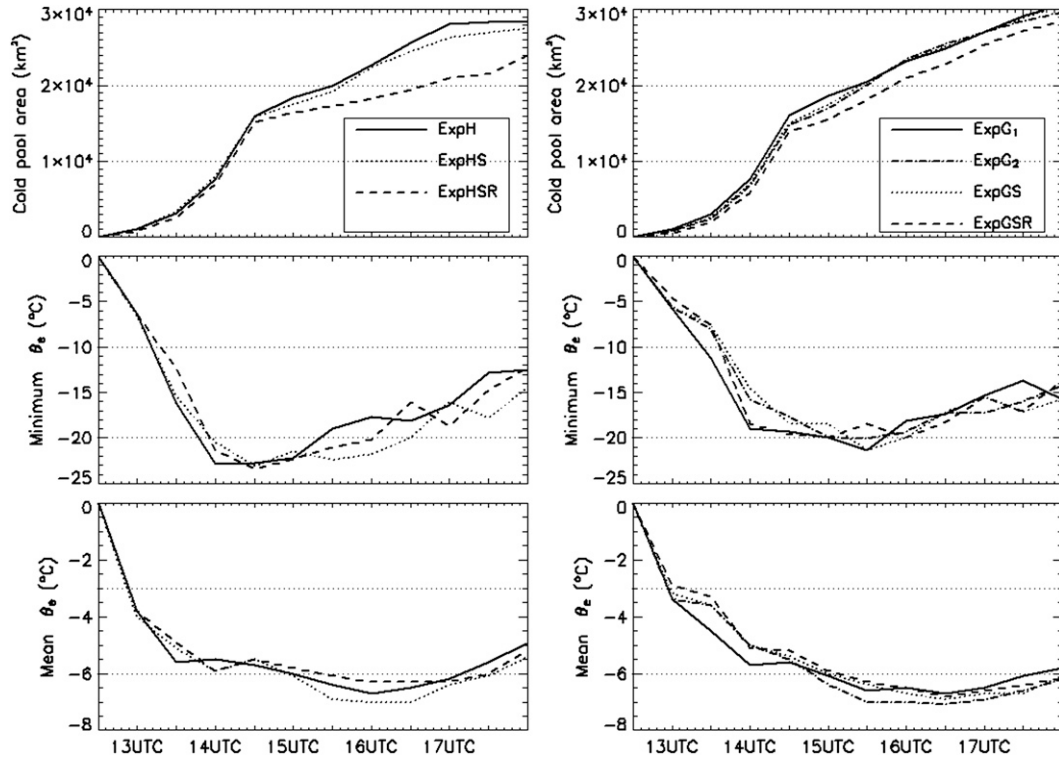


FIG. 11. (left) Hail- and (right) graupel-weighted experiments: (top) cold pool area ( $\text{km}^2$ ) evolution, (middle) evolution of the minimum equivalent potential temperature perturbation (K) within cold pools, and (bottom) evolution of the mean equivalent potential temperature perturbation (K) within cold pools. Cold pools are defined as areas with an equivalent potential temperature below  $-2$  K, compared to the mean value over the domain, excluding water areas.

respective counterparts with the original snow size distribution formulations (Figs. 5a and 5b; Table 3). The impact of these experiments on both precipitation efficiency and thermodynamics (not shown) is virtually negligible.

As for the snow variable, the intercept parameter of rain is kept constant in most one-moment bulk microphysical schemes, while it is known to vary significantly from observational data (e.g., Waldvogel 1974). Therefore, experiments ExpHS and ExpGS were further modified to include a mixing-ratio-dependent rain intercept parameter (ExpHSR and ExpGSR). From the analysis of 2D video disdrometer data, Zhang et al. (2008) found the intercept parameter of the rain size distribution to increase as the rain mixing ratio increased, leading to relatively larger (and hence faster) drops at small rain mixing ratios as compared to distributions with a fixed Marshall and Palmer (1948) intercept parameter. In our experiments, this modification leads to a significant reduction (about 15%) in the accumulated surface precipitation and maximum rain rate (Figs. 5a–d; Table 3). From Fig. 3a it is clear that at high rain mixing ratios, the mixing-ratio-dependent rain fall speeds are reduced by about 20%. This explains why maximum rain rates are reduced in this case.

However, it is odd that the accumulated total precipitation is also reduced, as there is no change in PE (Table 3) and updraft intensity is not clearly diminished (Figs. 13a and 13b). Taking a look at the cold pool characteristics reveals the likely reason for the decreased surface rain amounts, however (Figs. 11a and 11b). Cold pools in the experiments having a diagnosed rain intercept are consistently smaller than cold pools in the other experiments. From Fig. 3a, it is clear that rain sedimentation velocities are significantly increased for small mixing ratios and decreased for large mixing ratios, leaving less time for evaporation near the edges of storms and more time for evaporation in the high intensity cores. Furthermore, as the rain intercept parameter decreases with lower mixing ratios, the abundance of small drops decreases. Hence, fewer small drops and a smaller surface area–volume ratio further lead to reduced evaporation at the cold pool edges. This effectively shrinks the cold pool areas, while the inner parts remain as cold as compared to the experiments with constant rain intercepts (Figs. 11a and 11b). This finding is consistent with the recent findings of Dawson et al. (2010) and Li et al. (2009). As updrafts are forced on the frontal outflow boundary of

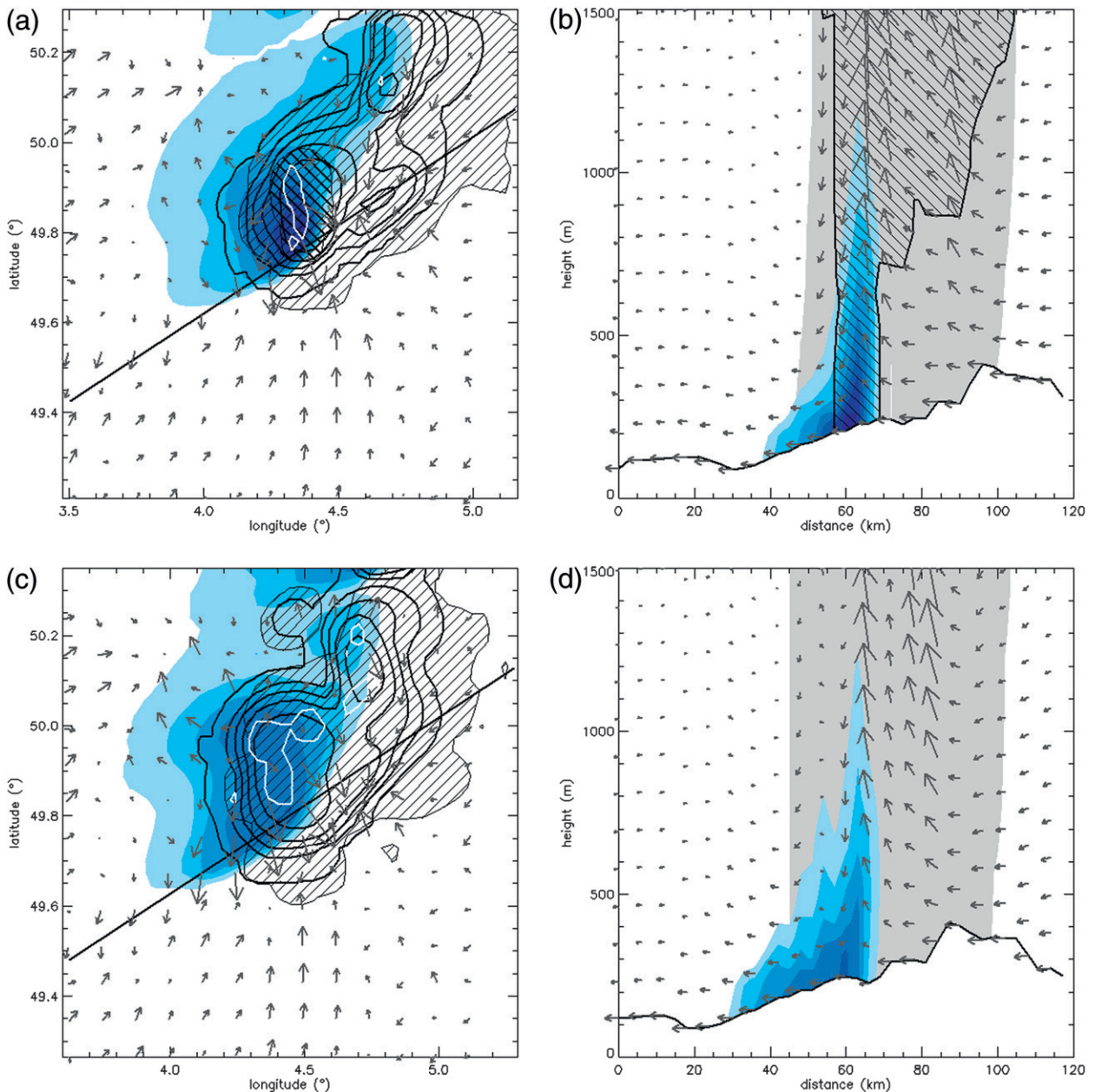


FIG. 12. (left) Horizontal and (right) vertical storm cross section for (top) ExpH and (bottom) ExpG<sub>1</sub>. Horizontal cross sections: Blue shading indicates the perturbation equivalent potential temperature from the average mean equivalent potential temperature within the panel domain ( $-3\text{-K}$  increment). Hatched areas denote the maximum cloud boundary, and heavy contours denote rain mixing ratio at the first level above the surface (contours at  $1.0 \times 10^{-5}$ ,  $1.0 \times 10^{-4}$ ,  $2.5 \times 10^{-4}$ ,  $5.0 \times 10^{-4}$ , and  $1.0 \times 10^{-3} \text{ kg kg}^{-1}$ ). Heavily hatched area in (a) indicates the area with hail reaching the surface, and white contour denotes the area with strongest downdrafts. Arrows indicate the deviation of surface wind vector from the mean wind vector in the panel area. Vertical cross sections: Cross sections are taken along the mean wind vector and intersecting the largest equivalent potential temperature perturbation. Blue shading indicates the perturbation of the equivalent potential temperature from the average mean equivalent potential temperature within the panel domain ( $-3\text{ K}$  increment). Gray shading indicates the area with rain mixing ratios above  $1.0 \times 10^{-5} \text{ kg kg}^{-1}$ , and hatched area denotes hail mixing ratios above  $1.0 \times 10^{-5} \text{ kg kg}^{-1}$ . Arrows indicate the deviation of the wind vector from the mean wind vector in the panel area.

propagating storms and the outflow area shrinks, storms tend to shrink too, eventually leading to storms having a similar intensity but smaller size as compared to the other experiments.

## 5. Summary and conclusions

In this research, a systematic setup was followed to investigate the influence of modified size distribution

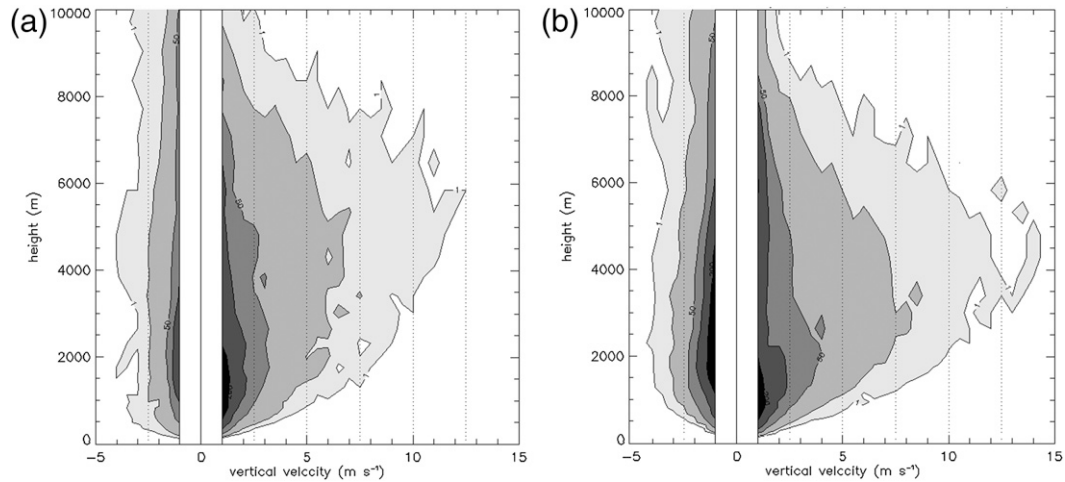


FIG. 13. As in Fig. 8, but for (a) ExpHSR and (b) ExpGSR.

assumptions of rain, snow, and hail within a bulk one-moment microphysics scheme on microphysical and thermodynamical aspects of deep moist convection. The impact of modifying the size distribution assumptions of the largest precipitating ice (hail–graupel) species, snow, and rain has been explored for a long-lived low-topped supercell case over Belgium.

Implementing an intercept parameter and density, typical for graupel instead of those typical for large-hail, leads to increased surface precipitation, in contrast to earlier findings by, for example, GSR04. It was found that although precipitation efficiency is decreased in the graupel-weighted experiment, thermodynamical heating due to enhanced freezing processes yields stronger updrafts, more condensation, and more intense storms. Implementing a more sophisticated formulation for the graupel variable, taking into account the empirical relations found by Locatelli and Hobbs (1974) for the calculation of the slope parameter and the fall velocity, yields even lower precipitation efficiencies but also more vigorous updrafts. In the end, surface precipitation was only slightly diminished by the more advanced representation of graupel, showing that experimental design is probably not the main reason for the different responses found in previous studies. While GSR04 suggested that the decrease of surface precipitation with decreasing graupel size could be related to the strength of the vertical wind shear, we could show that this response is also strongly dependent on storm depth. The thermodynamic atmospheric conditions in our simulations provoked the development of low-topped, rather shallow, supercell storms, while much deeper storms were simulated in most previously conducted studies. This left much more time for graupel sublimation and effectively reduced the precipitation efficiency in those simulations. In simulations by, for

example, GSR04, more favorable thermodynamics due to additional latent heating could not catch up with the decreased precipitation efficiency, while this was obviously the case in our simulations.

Experiments implementing more realistic size distribution assumptions for the snow species, including a temperature-dependent intercept parameter and the use of empirical mass–diameter relations for the calculation of the slope parameter, did not affect moist processes or surface precipitation significantly. Somewhat more snow was present in the simulations with modified size distribution assumptions, but this was not sufficient to impact precipitation efficiency or the thermodynamics of the storms. Implementing a mixing-ratio-dependent intercept parameter of the rain size distribution led to the most significant decrease in surface precipitation, although still modest (15%) and without solving the positive precipitation bias. This could not be related to changes in the precipitation efficiency or thermodynamics, but a mechanism was proposed by which surface cold pools strongly shrunk because of weaker rain evaporation at the cold pool boundaries. As updrafts were forced on the frontal edge of propagating evaporative cold pools, storm size tended to shrink as well, leading to decreased accumulated surface precipitation amounts.

This paper addressed a number of questions raised by previous research and generally showed that size distribution assumptions of one-moment microphysics schemes significantly affect the latent heat release, the precipitation formation process, and cold pool dynamics during strong precipitation events. In-depth research, including detailed observations of these aspects, is indispensable to understanding how more advanced microphysics schemes with enhanced computational demand could improve each of

these single aspects affecting the quantitative precipitation forecast.

*Acknowledgments.* This research was carried out in the framework of the QUEST-B project, funded by the Flemish Fund for Scientific Research (FWO-Vlaanderen). Furthermore, we would like to acknowledge the Center for Analysis and Prediction of Storms (CAPS) of Oklahoma University for providing the ARPS source code online. This research is conducted utilizing high-performance computational resources provided by the University of Leuven (available online at <http://ludlit.kuleuven.be/hpc>).

#### REFERENCES

- Cohen, C., and E. W. McCaul, 2006: The sensitivity of simulated convective storms to variations in prescribed single-moment microphysics parameters that describe particle distributions, sizes, and numbers. *Mon. Wea. Rev.*, **134**, 2547–2565.
- Dawson, D. T., M. Xue, J. A. Milbrandt, and M. K. Yau, 2010: Comparison of evaporation and cold pool development between single-moment and multimoment bulk microphysics schemes in idealized simulations of tornadic thunderstorms. *Mon. Wea. Rev.*, **138**, 1152–1171.
- Deng, A., and D. R. Stauffer, 2006: On improving 4-km mesoscale model simulations. *J. Appl. Meteor. Climatol.*, **45**, 361–381.
- Federer, B., and A. Waldvogel, 1975: Hail and raindrop size distributions from a Swiss multicell storm. *J. Appl. Meteor.*, **14**, 91–97.
- Ferrier, B. S., 1994: A double-moment multiple-phase four-class bulk ice scheme. Part I: Description. *J. Atmos. Sci.*, **51**, 249–280.
- Gilmore, M. S., J. M. Straka, and E. N. Rasmussen, 2004: Precipitation uncertainty due to variations in precipitation particle parameters within a simple microphysics scheme. *Mon. Wea. Rev.*, **132**, 2610–2627.
- Goudenhoofd, E., and L. Delobbe, 2009: Evaluation of radar-gauge merging methods for quantitative precipitation estimates. *Hydrol. Earth Syst. Sci.*, **13**, 195–203.
- Groenemeijer, P. H., and A. van Delden, 2007: Sounding-derived parameters associated with large hail and tornadoes in the Netherlands. *Atmos. Res.*, **83**, 473–487.
- Gunn, K. L. S., and J. S. Marshall, 1958: The distribution with size of aggregate snowflakes. *J. Meteor.*, **15**, 452–461.
- Houze, R. A., P. V. Hobbs, P. H. Herzegh, and D. B. Parsons, 1979: Size distributions of precipitation particles in frontal clouds. *J. Atmos. Sci.*, **36**, 156–162.
- Kain, J. S., and J. M. Fritsch, 1993: Convective parameterization for mesoscale models: The Kain–Fritsch scheme. *The Representation of Cumulus Convection in Numerical Models*, Meteor. Monogr., No. 24, Amer. Meteor. Soc., 165–170.
- , and Coauthors, 2008: Some practical considerations regarding horizontal resolution in the first generation of operational convection-allowing NWP. *Wea. Forecasting*, **23**, 931–952.
- Khain, A., A. Pokrovsky, and I. Sednev, 1999: Some effects of cloud-aerosol interaction on cloud microphysics structure and precipitation formation: Numerical experiments with a spectral microphysics cloud ensemble model. *Atmos. Res.*, **52**, 195–220.
- Kogan, Y. L., 1991: The simulation of a convective cloud in a 3D model with explicit microphysics. Part I: Model description and sensitivity experiments. *J. Atmos. Sci.*, **48**, 1160–1189.
- Li, X., W.-K. Tao, A. P. Khain, J. Simpson, and D. E. Johnson, 2009: Sensitivity of a cloud-resolving model to bulk and explicit bin microphysical schemes. Part II: Cloud microphysics and storm dynamics interactions. *J. Atmos. Sci.*, **66**, 22–40.
- Lin, Y.-L., R. D. Farley, and H. D. Orville, 1983: Bulk parameterization of the snow field in a cloud model. *J. Climate Appl. Meteor.*, **22**, 1065–1092.
- Liu, J. Y., and H. D. Orville, 1969: Numerical modeling of precipitation and cloud shadow effects on mountain-induced cumuli. *J. Atmos. Sci.*, **26**, 1283–1298.
- Locatelli, J. D., and P. V. Hobbs, 1974: Fall speeds and masses of solid precipitation particles. *J. Geophys. Res.*, **79**, 2185–2197.
- Marshall, J. S., and W. M. Palmer, 1948: The distribution of raindrops with size. *J. Meteor.*, **5**, 165–166.
- McCumber, M., W.-K. Tao, J. Simpson, R. Penc, and S.-T. Soong, 1991: Comparison of ice-phase microphysical parameterization schemes using numerical simulations of tropical convection. *J. Appl. Meteor.*, **30**, 985–1004.
- Milbrandt, J. A., and M. K. Yau, 2005: A multimoment bulk microphysics parameterization. Part II: A proposed three-moment closure and scheme description. *J. Atmos. Sci.*, **62**, 3065–3081.
- , and —, 2006: A multimoment bulk microphysics parameterization. Part III: Control simulation of a hailstorm. *J. Atmos. Sci.*, **63**, 3114–3136.
- Morrison, H., G. Thompson, and V. Tatarskii, 2009: Impact of cloud microphysics on the development of trailing stratiform precipitation in a simulated squall line: Comparison of one- and two-moment schemes. *Mon. Wea. Rev.*, **137**, 991–1007.
- Noilhan, J., and S. Planton, 1989: A simple parameterization of land surface processes for meteorological models. *Mon. Wea. Rev.*, **117**, 536–549.
- Ovtchinnikov, M., and Y. L. Kogan, 2000: An investigation of ice production mechanisms in small cumuliform clouds using a 3D model with explicit microphysics. Part I: Model description. *J. Atmos. Sci.*, **57**, 2989–3003.
- Seifert, A., and K. D. Beheng, 2006: A two-moment cloud microphysics parameterization for mixed-phase clouds. Part 2: Maritime vs. continental deep convective storms. *Meteor. Atmos. Phys.*, **92**, 67–82.
- Stein, U., and P. Alpert, 1993: Factor separation in numerical simulations. *J. Atmos. Sci.*, **50**, 2107–2115.
- Sui, C. H., X. Li, and M.-J. Yang, 2007: On the definition of precipitation efficiency. *J. Atmos. Sci.*, **64**, 4506–4513.
- Sun, W.-Y., and C.-Z. Chang, 1986: Diffusion model for a convective layer. Part I: Numerical simulation of convective boundary layer. *J. Climate Appl. Meteor.*, **25**, 1445–1453.
- Thompson, G., P. R. Field, R. M. Rasmussen, and W. D. Hall, 2008: Explicit forecasts of winter precipitation using an improved bulk microphysics scheme. Part II: Implementation of a new snow parameterization. *Mon. Wea. Rev.*, **136**, 5095–5115.
- van den Heever, S. C., and W. R. Cotton, 2004: The impact of hail size on simulated supercell storms. *J. Atmos. Sci.*, **61**, 1596–1609.
- Waldvogel, A., 1974: The  $N_0$  jump of raindrop spectra. *J. Atmos. Sci.*, **31**, 1067–1078.
- Weisman, M. L., C. Davis, W. Wang, K. W. Manning, and J. B. Klemp, 2008: Experiences with 0–36-h explicit convective forecasts with the WRF-ARW model. *Wea. Forecasting*, **23**, 407–437.

- Wisner, C., H. D. Orville, and C. Myers, 1972: A numerical model of a hail-bearing cloud. *J. Atmos. Sci.*, **29**, 1160–1181.
- Xue, M., 2000: High-order monotonic numerical diffusion and smoothing. *Mon. Wea. Rev.*, **128**, 2853–2864.
- , K. K. Droegemeier, and V. Wong, 2000: The Advanced Regional Prediction System (ARPS)—A multi-scale nonhydrostatic atmospheric simulation and prediction model. Part I: Model dynamics and verification. *Meteor. Atmos. Phys.*, **75**, 161–193.
- , and Coauthors, 2001: The Advanced Regional Prediction System (ARPS)—A multi-scale nonhydrostatic atmospheric simulation and prediction tool. Part II: Model physics and applications. *Meteor. Atmos. Phys.*, **76**, 143–165.
- Zhang, G., M. Xue, Q. Cao, and D. Dawson, 2008: Diagnosing the intercept parameter for exponential raindrop size distribution based on video disdrometer observations: Model development. *J. Appl. Meteor. Climatol.*, **47**, 2983–2992.

Copyright of Monthly Weather Review is the property of American Meteorological Society and its content may not be copied or emailed to multiple sites or posted to a listserv without the copyright holder's express written permission. However, users may print, download, or email articles for individual use.